Engineering Inorganic Nanoemulsions/Nanoliposomes by Fluoride-Silica Chemistry for Efficient Delivery/Co-Delivery of Hydrophobic Agents

Yu Chen, Yu Gao, Hangrong Chen, Deping Zeng, Yaping Li,* Yuanyi Zheng, Faqi Li, Xiufeng Ji, Xia Wang, Feng Chen, Qianjun He, Linlin Zhang, and Jianlin Shi**

A novel drug-formulation protocol is developed to solve the delivery problem of hydrophobic drug molecules by using inorganic mesoporous silica nanocapsules (IMNCs) as an alternative to traditional organic emulsions and liposomes while preserving the advantages of inorganic materials. The unique structures of IMNCs are engineered by a novel fluoride-silica chemistry based on a structural difference-based selective etching strategy. The prepared IMNCs combine the functions of organic nanoemulsions or nanoliposomes with the properties of inorganic materials. Various spherical nanostructures can be fabricated simply by varying the synthetic parameters. The drug loading amount of a typical highly hydrophobic anticancer drug-camptothecin (CPT) in IMNCs reaches as high as 35.1 wt%. The intracellular release of CPT from carriers is demonstrated in situ. In addition, IMNCs can play the role of organic nanoliposome (multivesicular liposome) in co-encapsulating and co-delivering hydrophobic (CPT) and hydrophilic (doxorubicin, DOX) anticancer drugs simultaneously. The co-delivery of multi-drugs in the same carrier and the intracellular release of the drug combinations enables a drug delivery system with efficient enhanced chemotherapeutic effect for DOX-resistant MCF-7/ADR cancer cells. The special IMNCs-based "inorganic nanoemulsion", as a proof-of-concept, can also be employed successfully to encapsulate and deliver biocompatible hydrophobic perfluorohexane (PFH) molecules for high intensity focused ultrasound (HIFU) synergistic therapy ex vivo and in vivo. Based on this novel design strategy, a wide range of inorganic material systems with similar "inorganic nanoemulsion or nanoliposome" functions will be developed to satisfy varied clinical requirements.

1. Introduction

More than forty percent of active anti-disease substances being screened by combinatorial screening programs possess hydrophobic nature.[1] Such a hydrophobic character makes them difficult to be directly developed as drug products for clinical translations because the low water solubility will strongly prevent them from being administrated through intravenous route and will result in low pharmacological bioavailability. Chemical modification of drug molecules by advanced organic/inorganic synthetic chemistry is the typical, commercial protocol used to make these hydrophobic drug molecules more water soluble. Such modifications, however, will unexpectedly result in the loss of anti-disease activity and significant alterations in the toxicological features of the drug molecules. For example, irinotecan, the derivative of highly hydrophobic anticancer drug-camptothecin (CPT) with improved water-soluble behavior, was found to exhibit significantly lowered cytotoxicity to cancer cells compared to initial CPT molecules.[2] Thus, alternative strategies to traditional chemical modifications for improved drug water solubility are highly recommended.

Dr. Y. Chen, Prof. H. Chen, Dr. X. Wang, Dr. F. Chen, Dr. Q. He, Dr. L. Zhang, Prof. J. Shi
State Key Laboratory of High Performance Ceramic and Superfine Microstructures
Shanghai Institute of Ceramics
Chinese Academy of Sciences
Shanghai, 200050, P. R. China
E-mail: hrchen@mail.sic.ac.cn; jlshi@sunm.shcnc.ac.cn
Dr. Y. Gao, Prof. Y. Li, Dr. X. Ji
Shanghai Institute of Materia Medica
Chinese Academy of Sciences
Shanghai, 201203, P. R. China
E-mail: ypli@mail.shcnc.ac.cn
Prof. D. Zeng, Prof. F. Li
State Key Laboratory of Ultrasound Engineering in Medicine Co-founded by Chongqing and the Ministry of Science and Technology
Chongqing Key Laboratory of Ultrasound in Medicine and Engineering
College of Biomedical Engineering
Chongqing Medical University
Chongqing, 400016, P. R. China
Prof. Y. Zheng
Second Affiliated Hospital of
Chongqing Medical University
Chongqing, 400010, P. R. China

DOI: 10.1002/adfm.201102052

Recently, nano-biotechnology has found the way to partially solve this problem by various material-based drug-formulation techniques,[3] among which organic systems such as surfactants or polymer-based emulsions or liposomes with separate hydrophobic and hydrophilic domains are the typical early representatives.[4] The low drug encapsulation efficiency and chemical/thermal instability of these organic drug delivery systems (DDSs), however, have largely impeded their further clinical application. Alternatively, inorganic material systems have attracted increasing attention in nano-biomedicine due to their high stability, excellent biocompatibility, and good degradability.[5] Tailoring the structures of inorganic bio-nanomaterials with similar functions to organic systems while preserving their unique features, such as high stability, could further promote nanomedical products into the clinical stage.

Herein, we would like to introduce a new concept of "inorganic nanoemulsions or nanoliposomes" based on inorganic mesoporous nanocapsules (designated as IMNCs) to achieve the functions of organic emulsions or liposomes, and in the meantime demonstrate the advantages of inorganic materials. As shown in **Figure 1**a, the IMNCs exhibit unique structural characteristics, such as large hollow interiors and mesoporous shells. It is known that a conventional organic nanoemulsion consists of two distinct separate parts, the hydrophobic core as the reservoir for water-insoluble agents and the hydrophilic surface enabling dispersion in water. In this respect, the unique structure of IMNCs enables them to play the same roles as a nanoemulsion for hydrophobic agents: the hollow core part functions as reservoirs for hydrophobic agents while the hydrophilic mesoporous shell guarantees the water dispersivity of the nanocarriers; thus, IMNCs can be regarded as inorganic nanoemulsions. In addition to the similar functions of IMNCs to organic nanoemulsion, another important organic drug delivery system, nanoliposomes, could be well-mimicked by IMNCs to introduce another important concept of "inorganic nanoliposomes" if the mesoporous silica shell is considered as the other reservoir for hydrophilic drugs. The organic nanoliposome (specifically the multivesicular liposome) is capable of enwrapping both hydrophobic and hydrophilic drugs simultaneously because of its unique micro/nano-structure. As shown in Figure 1b, the organic liposome consists of separate hydrophobic and hydrophilic domains, which act as the reservoirs for hydrophobic and hydrophilic agents, respectively. The IMNCs show similar structural characteristics: i) a large hollow interior that can function as the reservoir for hydrophobic agents, and, ii) a mesoporous silica shell with controllable thickness, hydrophilic inner/outer surface, tunable pore size, large surface area, and pore volume guarantees efficient encapsulation of hydrophilic agents.

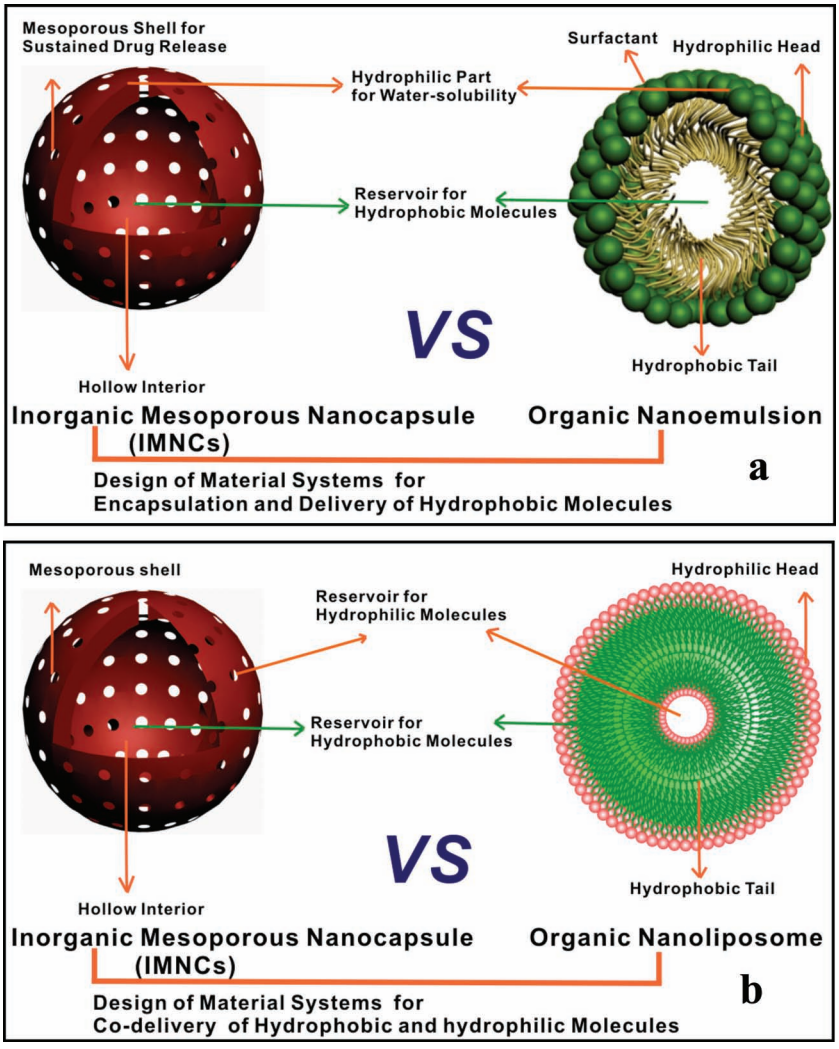

Figure 1. Comparisons and similarities of the microstructures and functionalities: a) between IMNCs and traditional organic nanoemulsions for encapsulating hydrophobic drug molecules and b) between IMNCs and organic nanoliposomes for the co-loading/co-delivery of hydrophobic and hydrophilic agents.

In this study, first we propose a new and controllable F^- ion-assisted etching strategy to engineer the structures of IMNCs based on a structural difference-based selective etching strategy and fluoride-silica chemistry.[6] Furthermore, the concept of "inorganic nanoemulsions" based on IMNCs was demonstrated by the successful and efficient encapsulation and intracellular delivery of hydrophobic anticancer drugs (CPT). In addition, IMNCs were introduced into a novel non-invasive therapeutic modality-high intensity focused ultrasound (HIFU) therapy by using such an "inorganic nanoemulsion" to encapsulate and deliver biocompatible but hydrophobic HIFU synergistic agent perfluorohexane (PFH) both ex vivo (bovine liver) and in vivo (rabbit). Last but not least, the concept of "inorganic nanoliposomes" based on IMNCs was illustrated by the successful co-encapsulation and co-delivery of hydrophobic (CPT) and hydrophilic (doxorubicin, DOX) anticancer drugs in IMNCs

simultaneously. The enhanced therapeutic effect of co-loaded drug combinations in IMNCs was demonstrated by the cytotoxicity promotion of the anticancer drug against drug resistant cells (MCF-7/ADR cells).

2. Results and Discussion

2.1. Fabrication of IMNCs Employing Structural Difference-Based Selective Etching Strategy Based on Fluoride-Silica Chemistry

The abundant silica chemistry endows the successful fabrication of silica-based nanomaterials with diverse structures, morphologies and compositions, making the exploration of related applications possible, such as in catalysis, separation, nanomedicine, chemical/biological sensing, optical device, etc.[7] Fine tuning of mesoporous silica nanostructures in nanoscale provides enormous chances for the preparation of silica-based materials with new structures and functions.[8] It is known that –Si–O–Si– bonds can be broken under alkaline conditions, and this mechanism has been successfully employed to prepare silica nanostructures with hollow interiors (e.g., by Na_2CO_3, ammonium, or NaOH etching).[6a,b,8b,9] However, such bond-breakage processes in an alkaline environment are reversible, together with the simultaneous bond-reformation process.[9b] This characteristic makes the synthetic procedure and material structures a little difficult to control, and usually brings in the unexpected by-products. Another important aspect of silica chemistry is the so-called "fluoride-silica" chemistry based on the dissolubility of silica by coordinating F^- ions to Si atoms that weakens the –Si–O–Si– bonds afterwards.[3d,10] This reaction is fast and irreversible, and might be employed as a general way to tune the silica nanostructures by the rational design in nanoscale (e.g., etching time, F^- ions concentration, and etching temperature).

In order to create the IMNCs by this special "fluoride-silica" chemistry, we prepared a composite solid silica core/mesoporous silica shell ($sSiO_2@mSiO_2$) structure in advance where the condensation/densification degrees of silica source in the core part are significantly lower than those in the shell according to our previous findings (**Figure 2**).[6a,b] Such a structural difference between the core and shell might result in the significant variations of structural stability under the same etching conditions. As shown in Figure 2, we anticipated that the F^- ions should be capable of breaking –Si–O–Si– bonds faster in the core part than in the shell by precisely controlling the etching process based on the the lower condensation/densification degree, e.g., more Si–OH or Si–OR bonds of silica in the core, thus the core part could be etched away prior to the shell, eventually leading to the formation of hollow silica nanostructures (Figure 2).

Monodispersed solid silica core/mesoporous silica shell ($sSiO_2@mSiO_2$) structured nanoparticles (NPs) with significant structural differences (e.g., condensation/densification degrees) between the core and shell were first fabricated by a stepwise coating procedure combined with the conventional Stöber process using the traditional long-chain silicon

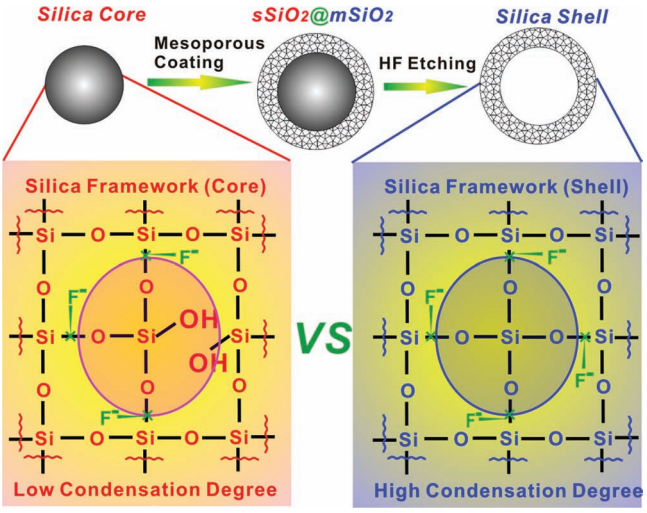

Figure 2. Schematic illustration of preparing structurally-different $sSiO_2@mSiO_2$ core/shell NPs and the corresponding microstructure comparisons between the core and shell of $sSiO_2@mSiO_2$ under attack by F^- ions. More Si–OH bonds are present in the silica core than in the framework of mesoporous shell because of the lower condensation/densification degree of silica core, resulting in the easier breakdown of the silica network in the core.

coupling agent octadecyltrimethoxysilane (C_{18}TMS) as the structural directing agents and tetraethyl orthosilicate (TEOS) as the silica source (**Figure 3**a,e).[6a,b] The chemical bonding at the core–shell interface was probably weaker than other parts, leading to the quick etching-away by F^- and the formation of rattle-type (or yolk-shell) $sSiO_2@Void@mSiO_2$ nanostructures (Figure 3b,f; 500 μL HF addition, 60 °C and 2 h etching). The solid silica core of $sSiO_2@mSiO_2$ were formed by the aggregation of sub-particles followed by further shell-growth on the initially formed silica NPs,[9b] so the inner part of the core is less dense and more porous than the outer part of the core, resulting in the faster etching away of the inner part and the formation of a special double-shelled silica structure (Figure 3c,g, 800 μL HF addition, 60 °C and 2 h etching). More F^- ions addition led to the complete removal of the core part of $sSiO_2@mSiO_2$ and subsequently the creation of entirely hollow interiors (Figure 3d,h; 900 μL HF addition, 60 °C and 2 h etching). The whole core evolution process for IMNCs is schematically illustrated in Figure 3i, including solid, rattle-type, double-shelled, and hollow stages. The more detailed structural information of mesoporous silica NPs at various stages of interior evolution could be acquired from contrast differences in the dark-field STEM images and linear/area element mapping of Si and O elements (Figure 3j–m and Figure S1 in the Supporting Information). The signal intensities of Si and O elements vary significantly in the linear and area element scanning zones where the signals decrease significantly when the representative black zone is scanned, further demonstrating the formation of hollow volumes by the F^- ions etching. The uniformity and spherical morphology of IMNCs could be directly observed from SEM images (Figure 3n), and the hollow nanostructure is evidenced by purposely selected broken spheres (Figure 3o).

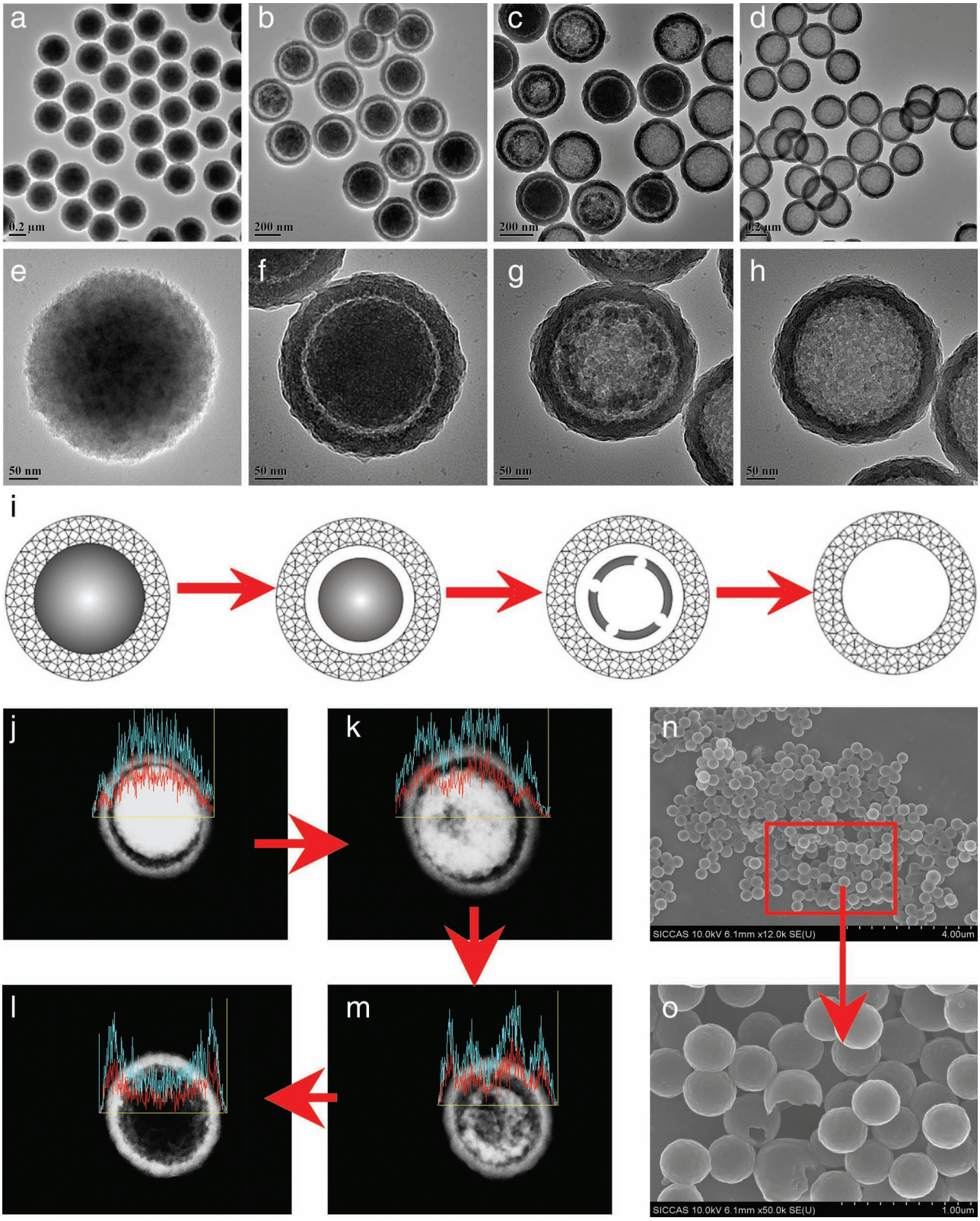

Figure 3. TEM images of $sSiO_2@mSiO_2$ (a) and IMNCs converted from $sSiO_2@mSiO_2$ by HF etching with the HF volumes of 500 μL (b), 800 μL (c) and 900 μL (d); TEM images (e–h) showing the structural evolution of the interior in $sSiO_2@mSiO_2$ from solid (e) to rattle-type (f), double-shelled (g), and hollow (h) structures; Schematic illustration (i) of the whole formation process of hollow interiors in $sSiO_2@mSiO_2$; Dark-field STEM images (j–m) at various stages of interior evolution in $sSiO_2@mSiO_2$, and the corresponding linear element mappings of Si and O elements in mesoporous silica nanostructures (the red: Si, and the green: O); SEM images of IMNCs at different magnifications (n,o).

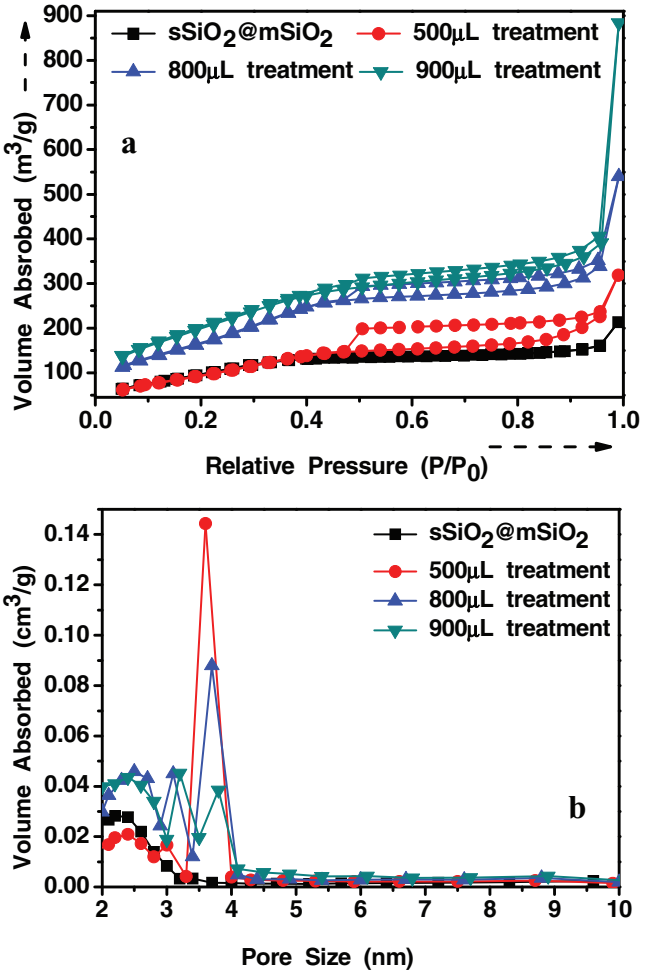

Figure 4. N_2 adsorption-desorption isotherms (a) and corresponding pore size distributions (b) of $sSiO_2@mSiO_2$, hollow mesoporous nanocapsules converted from $sSiO_2@mSiO_2$ by HF etching with the HF volumes of 500, 800 and 900 μL.

The well-defined pore structures, large surface area and high pore volume of the achieved mesoporous materials were characterized by typical N_2 adsorption–desorption techniques. The isotherms and corresponding pore size distribution curves are shown in **Figure 4**. The isotherms of the prepared samples exhibit the Langmuir IV hysteresis, indicating the well-defined mesoporous structure (Figure 4a). Compared to $sSiO_2@mSiO_2$ NPs, the IMNCs show the hierarchical pore size distributions where larger pores are dominant in the systems (Figure 4b and **Table 1**). The enlarged pores are due to the partial breakage of –Si–O–Si– bonds in the shell during the F^- etching process. Importantly, the surface area (from 375 to 756 $m^2\ g^{-1}$) and pore volume (from 0.33 to 1.37 $cm^3\ g^{-1}$) of IMNCs increase significantly after the etching (900 μL HF etching) compared to initial $sSiO_2@mSiO_2$ NPs (Table 1) due to the thinning of the inorganic wall in the shell and the creation of large hollow interiors, which guarantees their efficient encapsulation, delivery, and sustained-release of hydrophobic agents. In addition, our IMNCs show more advantages than recently reported hollow or

Table 1. Pore structural parameters (BET surface area: S_{BET}, pore volume: V_p and pore size) of $sSiO_2@mSiO_2$ and IMNCs converted from the $sSiO_2@mSiO_2$ by HF etching with the HF volumes of 500 (rattle), 800 (mixed), and 900 μL (hollow).

Sample	S_{BET} [$m^2\ g^{-1}$]	V_p [$cm^3\ g^{-1}$]	Pore Size [nm]
$sSO_2@mSiO_2$	375	0.33	2.4
Rattle (500 μL treatment)	365	0.49	2.4 & 3.0 & 3.6
Mixed (800 μL treatment)	642	0.83	2.5 & 3.1 & 3.7
Hollow (900 μL treatment)	756	1.37	2.4 & 3.2 & 3.8

rattle-type silica NPs, in which pores were totally created during the etching process, leading to broad pore size distributions, and low surface area and pore volume.[9a,10a,11] Comparatively, the pores in the present IMNCs were originally generated by the surfactants (long-chain silane coupling agents), and hereafter enlarged in the following etching process, resulting in well-defined pore size distribution, and correspondingly high surface area and pore volume.

2.2. IMNCs Functioning as "Inorganic Nanoemulsions" for Efficient Delivery of Hydrophobic Agents (CPT and PFH)

The function of IMNCs as "inorganic nanoemulsions" was first demonstrated by the encapsulation and intracellular delivery of hydrophobic anticancer drugs. CPT, a representative and most promising but hydrophobic anticancer drug, was selected as a typical model of hydrophobic agents. After impregnating IMNCs in CPT dimethyl sulfoxide (DMSO) solutions with varied concentrations (2, 4, and 8 mg mL^{-1}), the loading amount of CPT in IMNCs can be determined by thermo-gravimetric (TG) analysis. The drug weight losses were estimated to be 17.2%, 24.6%, and 35.1%, respectively, by subtracting the weight loss of physical water (**Figure 5**). Recently, Tang et al. employed rattle-type mesoporous silica NPs for the encapsulation and delivery

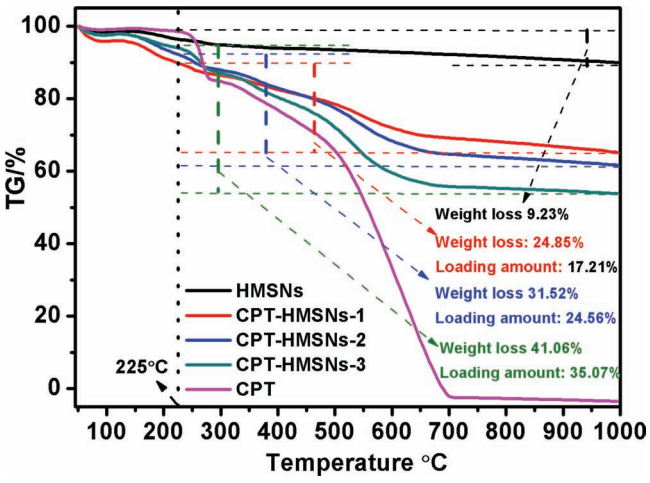

Figure 5. TG curves of IMNCs and CPT-IMNCs at different initial CPT impregnation concentrations (2, 4, and 8 mg mL^{-1}).

of the hydrophobic anticancer drug docetaxel.[3d] The loading amount could reach as high as 32%, further demonstrating the contribution of hollow interior for efficient drug loading. Our prepared IMNCs exhibit high CPT loading capability due to the contribution of large hollow interior, the volume of which leaves much more room for drug molecules. The IMNCs' hollow structure plays a similar role in loading hydrophobic agents to that of a metastable oil-in-water organic nanoemulsion, where hydrophilic mesoporous silica shell act as the interface between the oil (drug) drops in the hollow core and outer aqueous medium, or as part of hydrophilic medium.[6c]

To investigate the intracellular drug release behavior of CPT-loaded IMNCs, IMNCs were covalently conjugated with the typical organic fluorescent dye-rhodamine B (RhB) using simple silane conjugation chemistry (RhB/IMNCs), to make the carrier visible under confocal laser scanning microscope (CLSM) and facilitate the in situ observation of drug release from the support. As shown in **Figure 6**a–d and Figure S2 (in the Supporting Information), the efficient uptake of CPT-loaded RhB/IMNCs (CPT-RhB/IMNCs) by HeLa cells can be clearly observed from the red fluorescence emission of RhB/IMNCs. The strong blue fluorescence from CPT molecules is coincident with the red fluorescence from RhB/IMNCs, and much more blue fluorescence appears in the cytoplasm where the red fluorescence is absent, which indicates that IMNCs are capable of bringing CPT molecules into cancer cells via endocytosis and intracellularly releasing loaded CPT with time.[12] In addition, we further performed three-dimensional confocal fluorescent imaging of HeLa cells after uptake of CPT-RhB/IMNCs to demonstrate the intracellular delivery behavior of CPT-RhB/IMNCs (Figure 6e–g). The pink fluorescence signal (Figure 6g) comes from the superposition of red (RhB in Figure 6e) and blue (CPT in Figure 6f) fluorescences, further suggests that RhB/IMNCs could bring CPT into cells. The in vitro CPT release profiles in PBS and DMSO solutions were measured, from which it can be found that the CPT releasing from IMNCs exhibits a typical sustained profile (Figure S3). Only a small amount of CPT was released into PBS (6.9% in 48 h) because of the hydrophobic nature of CPT molecules, while the release of CPT in hydrophobic medium (DMSO) is much faster (39.2% in 48 h). No significant initial burst releases of CPT were detected, indicating the very limited amount of physically adsorbed CPT molecules on the outer surface of the carriers. There exist at least two following situations under which the intracellular release of hydrophobic CPT molecules encapsulated in the carriers can be expected. First, although the CPT solubility in aqueous condition is very low, the hydrophobic CPT still could dissolve, though very slowly, in aqueous solution, under the great concentration gradient of CPT between in the carrier and in the solutions to make small amount of drugs diffuse outside the mesopores. Second, some parts of the cell, such as cell membranes, are hydrophobic, which can promote the release of the hydrophobic drugs from mesopores under this special hydrophobic condition.

We further introduce this novel IMNCs-based "inorganic nanoemulsion" as the vehicle to encapsulate and deliver highly biocompatible but hydrophobic perfluorohexane (PFH) molecules for high intensity focused ultrasound (HIFU) synergistic therapy. As a non-invasive therapeutic mode, HIFU can deposit and convert acoustic energy into heat in a local volume

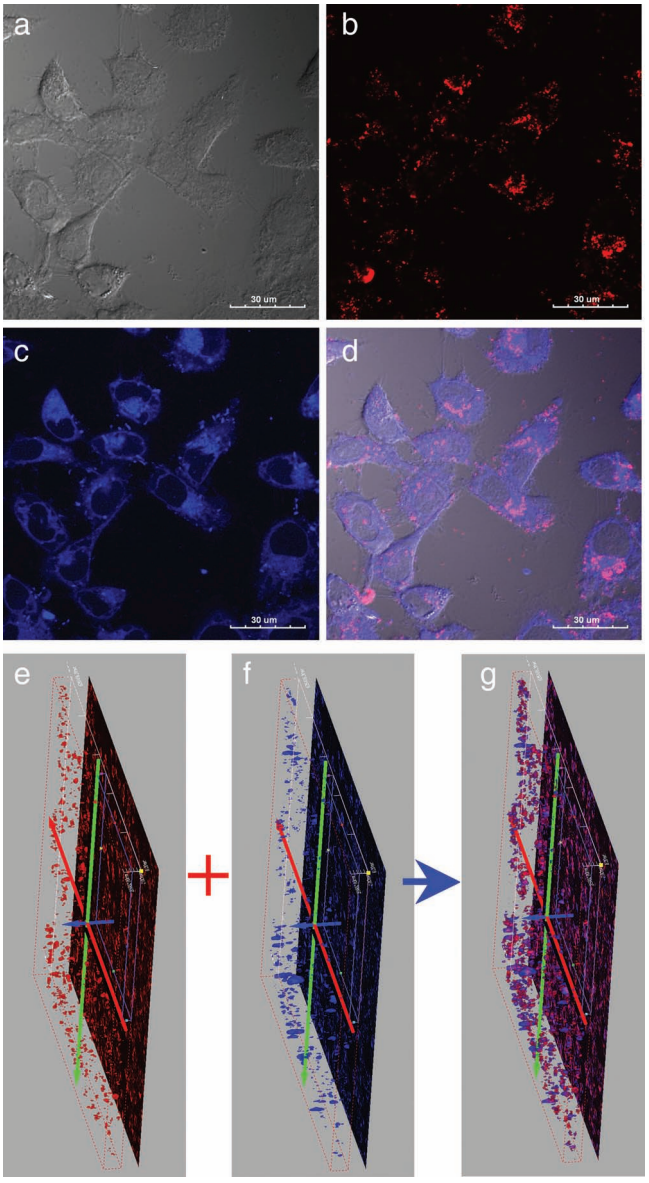

Figure 6. CLSM images (a–d) of HeLa cells incubated with CPT-loaded RhB/IMNCs (CPT concentrations: 15 μg mL^{-1}) for 3 h (a: bright field image, b: red channel, c: blue channel, and d: merged image of a, b, and c); Three-dimensional fluorescence reconstruction (e–g) of HeLa cells after uptaking CPT-loaded RhB/IMNCs (e: red channel, f: blue channel, and g: merged image of e and f) to directly observe intracellular delivery of CPT by the IMNCs drug vehicles.

to rapidly raise the tissue temperature. Therefore, malignant lesions could be destroyed by hyperthermia under the ultrasound imaging monitoring outside (**Figure 7**a).[13] However, the therapeutic efficiency of HIFU is unfortunately not high enough when it reaches deep organs, where higher ultrasound energy supply is necessary than at epidermal tissues. The increased ultrasound energy could, undesirably, damage the normal tissues in the acoustic propagation channels. This contradiction might be partially solved by recently developed nanotechnologies. We employed IMNCs, as a proof-of-concept, to load and deliver highly hydrophobic PFH molecules with low

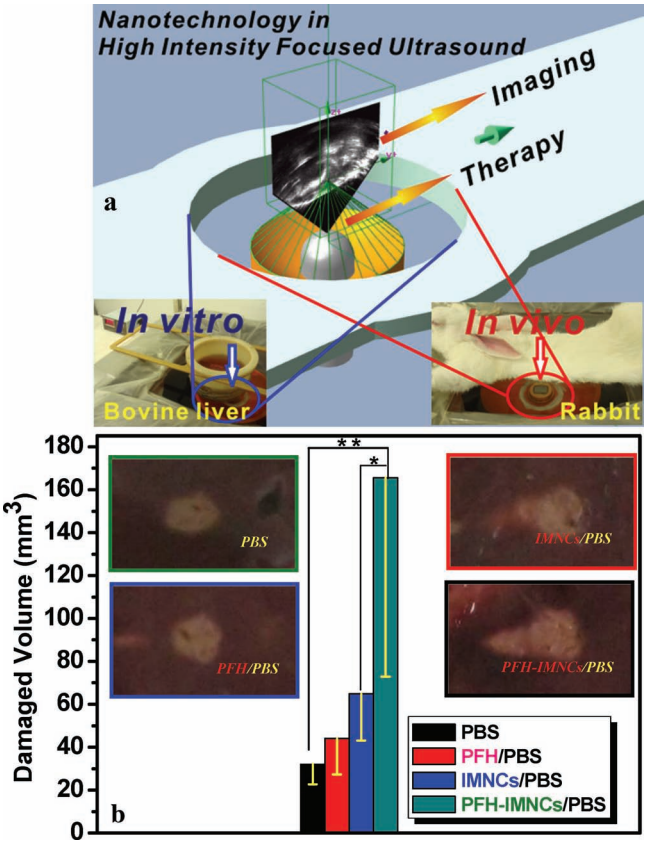

Figure 7. a) Schematic illustration of the high intensity focused ultrasound (HIFU) therapeutic principle. The HIFU radiates to the targeted site of the body and the process is monitored by the outside ultrasound imaging. The ex vivo experiment was conducted using bovine liver as a radiation substrate (left digital picture) while the in vivo experiment was carried out using rabbits as a model animal (the right digital picture); b) Coagulated tissue volume of bovine liver by the intra-tissue injection of different agents such as PBS (200 μL), PFH/PBS (200 μL), IMNCs/PBS (200 μL), and PFH-IMNCs/PBS (200 μL) under the same irradiation power and duration (150 W cm^{-2}, 5 s; $*P < 0.1$, $**P < 0.05$). Insets in (b) are the macroscopic appearances of bovine liver tissues exposed to HIFU with or without using the synergistic agents. The necrotic tissue is brighter, as can be easily distinguished from their unaffected surroundings.

boiling point, which was used and defined as the "synergistic agent" to improve HIFU therapeutic efficiency.

Typically, HIFU can destroy live tissue non-invasively by intrinsic hyperthermia, and its therapeutic efficiency has been reported improved by using organic microbubbles.[14] However, inorganic NPs show superior advantages over microbubbles because of their much more suitable size and higher stability than microbubbles. It has been reported that cell targeting outside the capillaries requires agent sizes of less than 700 nm to enable possible escape through the special large pores that are present in the leaky vasculature of a tumor.[15] Obviously, the sizes of microbubbles (several micrometers) are larger than this size limitation. The HIFU synergism using NPs might overcome the drawback of particle size of microbubbles. However, such research field has not been explored yet. Perfluorohexane (PFH), a highly biocompatible but hydrophobic contrast agent for ultrasound imaging with low boiling point (51–59 °C),[16] was selected to be encapsulated by IMNCs to synergize the HIFU therapy because it could be gasified by the HIFU hyperthermal effect.

Ex vivo experiments on bovine liver after the HIFU exposure with or without the synergistic agent were first conducted to assess the synergistic effect, and their therapeutic process was monitored by ultrasound imaging outside (Figure S4 in the Supportng Information). As shown in Figure 7b, the mean volume of the tissue coagulated by HIFU exposure varies significantly. The injections of both PFH/PBS and IMNCs/PBS exhibit higher therapeutic efficiency than the blank control (PBS), implying that PFH and IMNCs alone could have significant synergistic effect in HIFU therapy. The hydrophilic and highly dispersed IMNCs in aqueous solution could be well-retained in the tissue to change the tissue acoustic environment, while the hydrophobic PFH molecules cannot be dispersed in aqueous solution and will easily escape from the tissue. Therefore, the IMNCs/PBS revealed a slightly higher damage to the tissue than PFH/PBS did. Surprisingly, the mean volume of tissue coagulated by HIFU exposure in the group that received PFH-IMNCs/PBS (165.5 mm^3) was distinctively larger than those in the groups received PBS (32.1 mm^3), PFH/PBS (44.2 mm^3), and IMNCs/PBS (64.9 mm^3). The ex vivo results show that the IMNCs could efficiently encapsulate and deliver PHF molecules to remarkably enhance the therapeutic efficiency of HIFU therapy.

In order to assess the in vivo efficiency of PFH-encapsulated IMNCs as an HIFU synergistic agent, they were intravenously injected into rabbits through the ear vein. The NPs mostly accumulated into liver tissue because of the phagocytosis of the NPs by the reticuloendothelial systems (RES), which would be beneficial for the HIFU therapy of liver abnormalities such as liver cancer. The therapeutic efficiency of HIFU was observed and monitored by ultrasound imaging in a HIFU/Ultrasound Imaging equipment combination. **Figure 8** shows the ultrasound images of liver tissue before (left images) and after HIFU exposure (right images). The acoustic signal enhancement was all observed in liver tissue after the HIFU exposure because of the tissue coagulation effect caused by HIFU. However, the PFH-IMNCs/PBS sample exhibits much larger acoustic signal enhancement area than PBS, PFH/PBS, and IMNCs/PBS, indicating that PFH-IMNCs/PBS sample could greatly promote the absorption of acoustic energy and play an important role in improving the HIFU therapeutic efficiency in vivo. The IMNCs function as the reservoirs for hydrophobic PFH molecules and efficiently deliver the PFH into liver tissue, resulting in the much improved HIFU therapeutic efficacy. This novel application field further demonstrates the function of IMNCs as "inorganic nanoemulsion" for hydrophobic agents.

2.3. IMNCs Functionalize the "Inorganic Nanoliposomes" for Co-Encapsulation/Co-Delivery of Hydrophobic and Hydrophilic Anticancer Drugs

It is known that multi-drug combined chemotherapy has increasingly become a versatile strategy of great significance in clinical disease therapy because the encapsulation of multiple drugs into one system could bring forth enhanced therapeutic

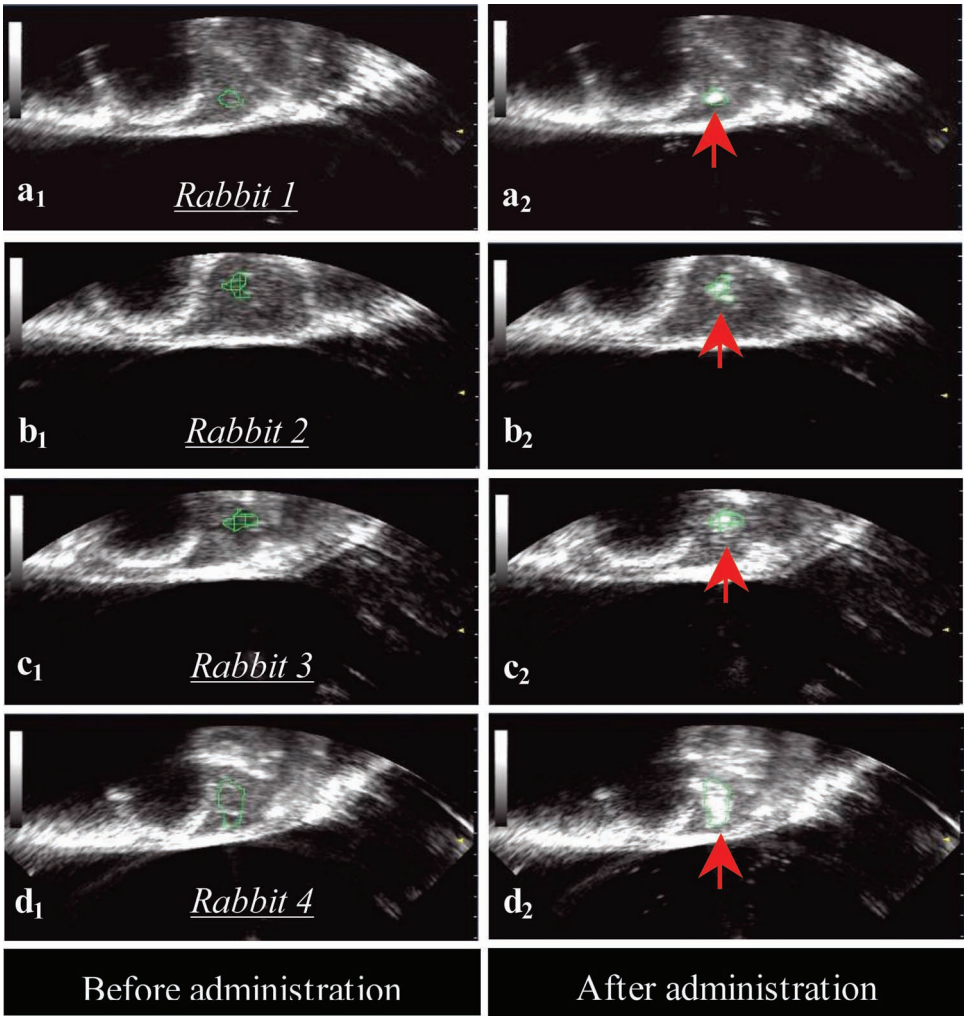

Figure 8. a–d) In vivo evaluation of therapeutic efficiency of HIFU by the intravenous injection of different agents into rabbits under the irradiation power of 150 W cm^{-2} and duration of 5 s by the ultrasound imaging monitoring outside (a_1 and a_2: PBS (2 mL), b_1 and b_2: PFH/PBS (2 mL), c_1 and c_2: IMNCs/PBS (2 mL), d_1 and d_2: PFH-IMNCs/PBS (2 mL)).

effect,[17] which has rarely been demonstrated in inorganic material systems, though the combinations of anticancer drugs and siRNA/DNA have been proposed and demonstrated to overcome the drug resistance of cancer cells.[18] Because of the unique structure of IMNCs, our developed "inorganic nanoliposome" is expected to realize the co-encapsulation of hydrophobic and hydrophilic small drug molecules into the carrier to achieve the substantially enhanced therapeutic goal.

To demonstrate this assumption, hydrophobic anticancer drug CPT and hydrophilic anticancer agent doxorubicin (DOX) were chosen as the model drugs to be loaded into IMNCs in sequence. The choice of such a two drug combination was based on the previous report that the combination of CPT and DOX could cause the remarkably enhanced cytotoxicities of anticancer drugs against cancer cells.[19] Besides, we chose DOX-resistant MCF-7/ADR cells to investigate whether CPT could add to the cytotoxicity of DOX against the drug-resistant cells, thus resulting in the enhanced therapeutic effect. Firstly, we investigated endocytosis behavior of IMNCs by MCF-7/ADR cancer cells and their subsequent intracellular location. As shown in **Figure 9**a_1–a_3 and S5 (see the Supporting Information), the strong red fluorescent spots representing RhB/IMNCs could be observed in the cytoplasm of the cells, verifying that the NPs could be uptaken by MCF-7/ADR cells. Three-dimensional confocal fluorescent image volumes of MCF-7/ADR cells further demonstrate that the fluorescent signal is originated from the cytoplasm rather than from the aggregates on the cell surface (Figure 9b_1–b_3). However, IMNCs NPs could not pass through the nuclear membrane to enter the nucleus, as demonstrated by the absence of red fluorescent signals of NPs in the nucleus.

The fluorescent nature of DOX (red fluorescence) and CPT (blue fluorescence) molecules facilitates the in situ observation of intracellular delivery and release of drugs from the carriers. As shown in **Figure 10**a_1–a_5 and S6 (see the Supporting Information), the blue and red fluorescences appear simultaneously in the cytoplasm of MCF-7/ADR cancer cells after 4 h co-incubation, and the pink fluorescence in the merged images of the blue and red further demonstrates that IMNCs could operate the intracellular co-delivery of CPT and DOX

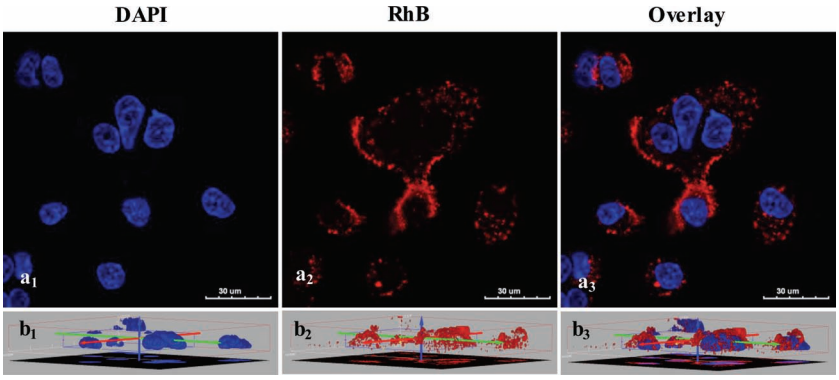

Figure 9. CLSM images (a_1–a_3) of MCF-7/ADR cells after co-incubation with RhB/IMNCs (50 μg mL^{-1}) for 4 h. After the incubation, the cell nuclei were stained with DAPI (blue fluorescence); Three-dimensional confocal fluorescence reconstructions (b_1–b_3) of nanoparticles endocytosed MCF-7/ADR cells to demonstrate the internalization and intracellular locations of NPs within cancer cells.

simultaneously (Figure 10a_4 and a_5). However, this fluorescence is associated with the cytoplasm rather than in the nucleus. A time-course (4, 12 and 24 h) fluorescent intensity enhancement of CPT and DOX in MCF-7/ADR cancer cells indicates the sustained and intracellular release of drugs from the carriers (Figure S7). With the longer incubation time, more CPT and DOX molecules could be found in the nucleus (12 and 24 h) from CLSM images (Figure 10b_1–b_5,10c_1–c_5, and S7–S8), indicating that DOX and CPT could be released in the cytoplasm and the released drugs could enter the nucleus afterwards.

To investigate the enhanced therapeutic effect caused by the co-delivery of CPT and DOX drug molecules, a traditional MTT assay was adopted to assess the cytotoxicity of free DOX, DOX-loaded IMNCs and DOX/CPT co-loaded IMNCs. IMNCs alone show very low cytotoxic effect by the MTT assessment (Figure S9 in the Supporting Information). As shown in **Figure 11**a and b, the MCF-7/ADR cells exhibit a high drug resistance to DOX molecules, demonstrated by the very low cytotoxicity of free DOX against MCF-7/ADR cells. When the drug was encapsulated into IMNCs, much enhanced cytotoxic effect of DOX-IMNCs could be found. The over-expression of multidrug efflux pumps such as P-glycoprotein (P-gp) is considered to be the main reason responsible for the drug-resistance of cancer cells.[19b] The higher cytotoxicity of DOX-IMNCs compared to free DOX is due to the bypassing of the P-gp induced efflux action by NPs because IMNCs are expected to be too large to be effluxed by P-gp. Importantly, DOX and CPT co-encapsulated IMNCs shows significantly higher cytotoxicity than either DOX-IMNCs or free DOX (Figure 11 and

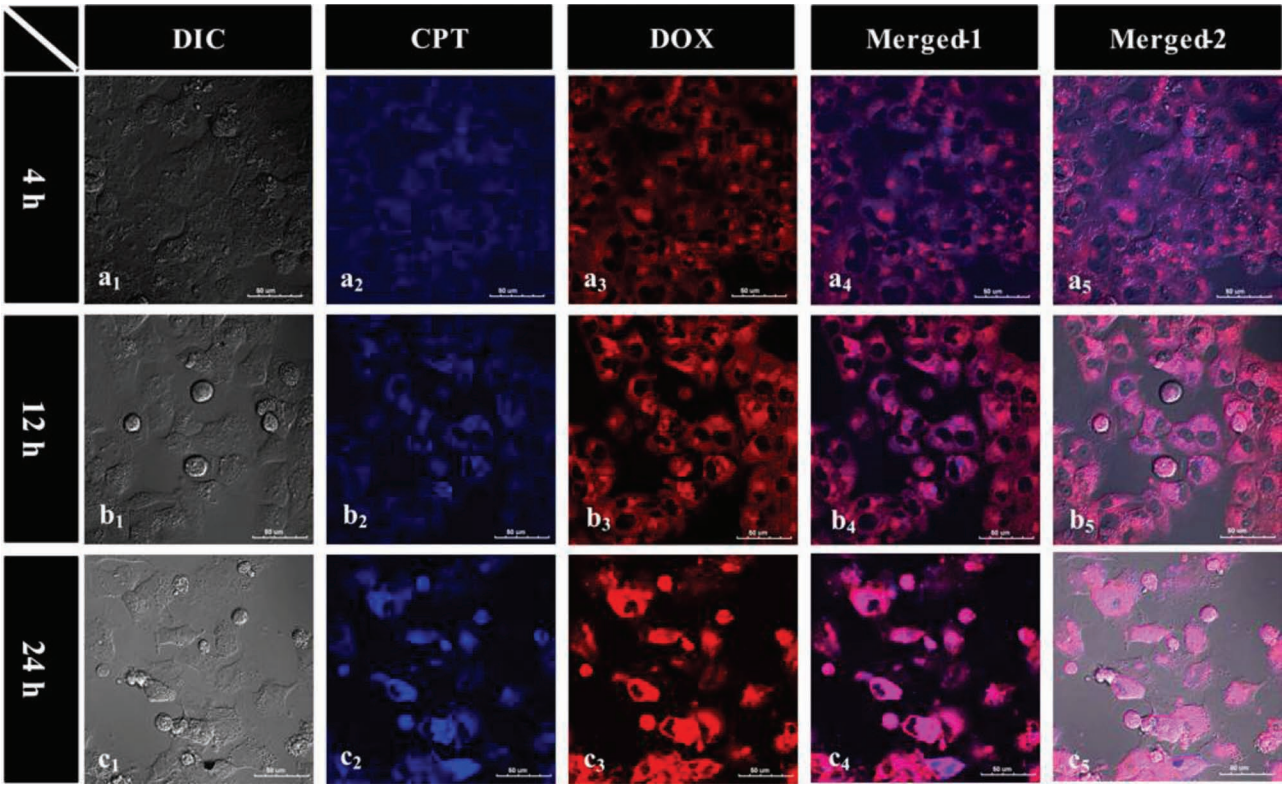

Figure 10. CLSM images of MCF-7/ADR cells incubated with DOX and CPT double-loaded IMNCs (DOX concentrations: 10 μg mL^{-1}) for different incubation time intervals (a_1–a_5: 4 h, b_1–b_5: 12 h, c_1–c_5: 24 h). Merged-1 are the superposed images of CPT and DOX channels, and merged-2 are those of DIC, CPT and DOX channels.

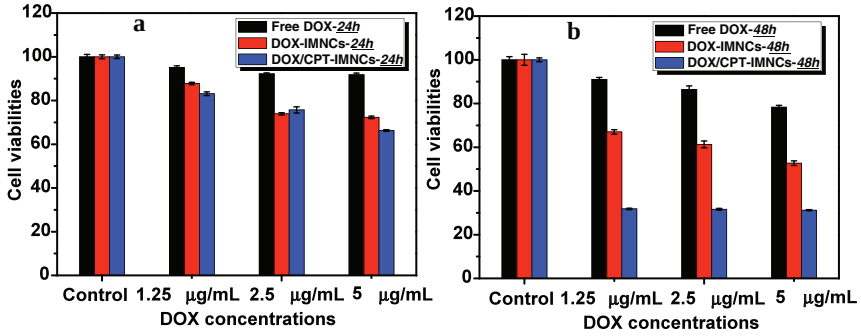

Figure 11. Cell viabilities of free DOX, DOX-IMNCs and DOX/CPT-IMNCs against MCF-7/ADR cells for different time intervals (a: 24 h, and b: 48 h). The control refers to the cells treated only with cell culture medium .

Figure S10, Supporting Information), demonstrating that the existence of CPT could effectively overcome the DOX resistance of MCF-7/ADR cancer cells. The anticancer efficiency of DOX/CPT-IMNCs is 62.8% (1.25 μg mL^{-1} DOX) in 48 h incubation, much higher than free DOX (21.7%, up to 5 μg mL^{-1} DOX) and DOX-IMNCs (47.3%, up to 5 μg mL^{-1} DOX), respectively. This enhanced anticancer effect can be attributed to the effects of bypassing the P-gp induced efflux action and CPT-enhanced cytotoxicity of the DOX/CPT-IMNCs drug delivery system.[19]

3. Conclusions

We have proposed a novel drug-formulation strategy to solve the problem of hydrophobicity of drug molecules by using engineered IMNCs as possible substitutes for traditional organic emulsions and liposomes, while preserving the advantages of inorganic materials. The major advantages of this strategy are based on its general applicability to most water-insoluble drugs, simplicity, and high efficiency. IMNCs were engineered by a novel fluoride-chemistry based on a structure difference-based selective etching strategy. The concepts of "inorganic nanoemulsions and nanoliposomes" based on IMNCs were successfully demonstrated by efficient encapsulation of hydrophobic anticancer drug (CPT) and simultaneous co-loading of hydrophobic (CPT) and hydrophilic (DOX) anticancer drugs, respectively. The intracellular release of CPT from IMNCs was demonstrated in vitro, and the co-delivery of CPT and DOX anticancer drugs in IMNCs brought forth the enhanced chemotherapeutic effect against DOX-resistant MCF-7/ADR cancer cells. Besides, this novel "inorganic nanoemulsion" was successfully introduced to encapsulate and deliver biocompatible but hydrophobic PFH molecules for HIFU synergistic therapy both ex vivo and in vivo. The present inorganic mesoporous nanocapsules provide a versatile platform for delivering hydrophobic agents, based on which a wide range of material systems with similar "inorganic nanoemulsion or nanoliposome" functionalities will be developed as, for example, the drug delivery systems or imaging agents for cancer diagnosis and therapy. In addition, the systematic investigations of the cytotoxicity of the achieved IMNCs on living bodies are required and under progress, which is necessary for their further clinical translations.

4. Experimental Section

Materials: Tetraethyl orthosilicate (TEOS), ethanol, ammonia solution (25–28%), hydrofluoric acid (HF, 40%) and dimethyl sulfoxide (DMSO) were obtained from Sinopharm Chemical Reagent Co. Octadecyltrimethoxysilane (C_{18}TMS) was purchased from Tokyo Chemical Industry Co., Ltd. Perfluorhexane (PFH, 99%) was purchased from Sigma-Aldrich. The anticancer drug doxorubicin (DOX) was provided by Beijing HuaFeng United Technology Co., Ltd. The anticancer drug camptothecine (CPT) was obtained from Knowshine (Shanghai) Pharmachemicals Inc. Phosphate buffer solution (PBS) was purchased from Shanghai Ruicheng Bio-Tech Co., Ltd. All regents were used without further purification. Deionized water was used in all experiments.

Preparation of IMNCs: The synthetic procedure was divided into two steps, including preparation of core/shell-structured $sSiO_2$@$mSiO_2$ NPs and subsequent etching in HF aqueous solution. Typically, ethanol (71.4 mL), water (10 mL) and ammonium solution (3.14 mL) were combined at 30 °C under stirring. TEOS (6 mL) was rapidly added into above solution and the stirring continued for 1 h at 30 °C in a water bath to form silica NPs. Subsequently, TEOS (5 mL) and C_{18}TMS (2 mL) were pre-mixed and rapidly added into the reaction media. The reaction proceeded for 1 h to produce $sSiO_2$@$mSiO_2$ core/shell NPs. The product was obtained by centrifugation and divided into six parts. Each part was dispersed into water (30 mL) by ultrasonic treatment. Then, certain amounts of HF solution (500, 800 or 900 μL) were added into $sSiO_2$@$mSiO_2$ aqueous solution dropwise at 60 °C under stirring (Caution: The reaction container cannot be glass because HF might react with the container). The etched product was recovered by centrifugation and washed with water for several times. The C_{18}TMS was removed by calcination at 550 °C for 6 h to create mesopores.

CPT Encapsulation in IMNCs: IMNCs (10 mg) were dispersed into CPT DMSO solutions (2 mL: 2, 4, or 8 mg mL^{-1}) by ultrasonic treatment. Then, the solution was shaken at 100 rpm at 37 °C for 24 h in the dark. The CPT-loaded IMNCs were obtained by centrifugation and dried under vacuum at room temperature, still under dark conditions. The in vitro CPT release experiment was conducted by loading of CPT-IMNCs (3 mg) into a dialysis bag (cutoff molecular weight: 3500), which was then put into the releasing medium (40 mL of PBS or DMSO) and the releasing process in a shaking table (100 rpm, 37 °C) was then monitored by UV-vis absorbance spectra at a wavelength of 366 nm.

PFH Encapsulation in IMNCs: Pre-dried IMNCs (100 mg) were put into a centrifuge tube (15 mL volume), followed by dropwise adding PFH liquid (200 μL). Then, the tube mouth was sealed tightly to avoid the evaporation of PFH molecules. The PFH-infiltrated IMNCs were subject to ultrasonic treatment for 30 s in an ice bath. PBS solution (10 mL) was added into PFH-IMNCs and the mixture was again subject to ultrasonic treatment to disperse PFH-IMNCs in PBS solution sufficiently after sealing the mouth tightly. The product was sealed tightly and stored at room temperature for further use.

DOX and CPT Co-Encapsulation in IMNCs: CPT-IMNCs were prepared by dispersion of IMNCs (10 mg) into CPT DMSO solution (2 mL,

2 mg mL^{-1}) for 24 h, followed by centrifugation and drying under vacuum at room temperature. For DOX loading, CPT-IMNCs (5 mg) were dispersed into DOX PBS solution (0.5 mg mL^{-1}). After stirring at room temperature for 24 h under dark conditions, the product was obtained by centrifugation and then dried under vacuum at room temperature.

Ex Vivo Evaluation of the Synergistic Effect of PFH-IMNCs in HIFU Therapy: The ex vivo assessment of synergistic effect of PFH-IMNCs in HIFU therapy was conducted by using degassed bovine livers as the model tissue. Typically, the bovine livers were cut into a cuboid shape and then put into a tank filled with degassed water. PFH-IMNCs in PBS solution (200 μL) was directly injected into the degassed bovine liver using a syringe (1 mL volume), and the injection site was monitored by an ultrasound imaging apparatus. When the PFH-IMNCs was injected quickly, the HIFU (irradiation power: 150 W cm^{-2}, irradiation time: 5 s) was imposed on the injection site immediately. Blank PBS solution (200 μL), IMNCs dispersed in PBS (200 μL) and PFH dispersed in PBS (200 μL) were employed as controls. Ultrasonic echo-signal was acquired by the software GrayVal 1.0 (Chongqing Haifu Technology, Chongqing, China). After exposure to HIFU, the volume of necrotic tissues in the degassed bovine were calculated by the following equation employing the Getcolorpixels software (Chongqing Haifu Technology, China): $V = (\pi/6)L_{max}W_{max}^2$, where L_{max} is the maximum length of coagulated tissue, and W_{max} the maximum width of coagulated tissue. Each sample was treated in triplicate.

In Vivo Evaluation of the Synergistic Effect of PFH-IMNCs in HIFU Therapy: The in vivo evaluation of the synergistic effect of PFH-IMNCs in HIFU therapy was carried out using New Zealand white rabbits (2.5–3.0 kg) as the model animal, which were provided by Laboratory Animals Center of Chongqing Medical University. The experiment was approved ethically and scientifically by the University and complied with Practice for Laboratory Animals in China. The rabbits were anesthetized and fixed in HIFU apparatus before the experiment. The PFH-IMNCs/PBS (2 mL) was administrated into the rabbit via the ear vein. After injection for 60 s, the HIFU (irradiation power: 150 W cm^{-2}, irradiation duration: 5 s) was imposed on the liver tissue immediately. The HIFU therapeutic procedure was monitored in situ by an ultrasound imaging apparatus combined with the HIFU therapy equipment. The blank PBS (2 mL), IMNCs dispersed in PBS (2 mL), and PFH dispersed in PBS (2 mL) were similarly administrated into other rabbits for control and comparison.

Cell Culture: HeLa cells and MCF-7/ADR cells were cultured in Dulbecco's modified Eagle's medium (DMEM) containing 10% fetal bovine serum (FBS), 100 units mL^{-1} penicillin and 100 μg mL^{-1} streptomycin. Cells were maintained at 37 °C in a humidified atmosphere of 5% CO_2 in air.

Confocal Laser Scanning Microscopy (CLSM) Observation of the Uptake of CPT-RhB/IMNCs and Intracellular Release of CPT in HeLa Cells: HeLa cells were seeded in a CLSM special culture dish with a cell density of 50%–60% and cultured in 5% CO_2 at 37 °C. The cell number in the CLSM-specific culture dish (3.5 cm) was 50×10^4 cells $dish^{-1}$. The cell number per millimeter is about 25 cells mm^{-1}. The CPT-RhB/IMNCs were dispersed into DMEM cell-culture media by ultrasonic treatment with the CPT concentration at 15 μg mL^{-1}. The cell-culture media of HeLa cells was replaced with DMEM containing CPT-RhB/IMNCs NPs (2 mL, 15 μg mL^{-1} of CPT). After co-incubation for 3 h, the cells were washed with PBS three times to remove the not-uptaken NPs. CLSM images were then acquired (FV 1000, Olympus, Japan).

CLSM Observation of the Uptake of RhB/IMNCs by MCF-7/ADR Cells: MCF-7/ADR cells were seeded in a CLSM-special culture dish with a cell density of 50%–60% and cultured in 5% CO_2 at 37 °C. The RhB/IMNCs were dispersed into DMEM cell-culture media by ultrasonic treatment at a concentration of 50 μg mL^{-1}. The cell-culture media of MCF-7/ADR cells was replaced with DMEM containing RhB/IMNCs NPs (2 mL, 50 μg mL^{-1}). After the co-incubation for 4 h, the cells were washed with PBS three times and the nuclei were stained by DAPI (Cell Apoptosis DAPI Detection Kit, KeyGEM). The CLSM images were acquired in CLSM (FV 1000, Olympus, Japan) and the three dimensional fluorescence reconstruction of nanoparticle-endocytosized cells were conducted by serial layer scanning of cells along the *Z*-axis and 3D reconstruction of scanned fluorescence images.

CLSM Observation of the Uptake of DOX/CPT-IMNCs and Intracellular Release of DOX and CPT in MCF-7/ADR Cells: DOX/CPT-IMNCs were dispersed into DMEM cell-culture media with a DOX concentration of 10 μg mL^{-1}. Then, DMEM (2 mL) containing DOX/CPT-IMNCs was added into a CLSM-specific culture dish of seeded MCF-7/ADR cells with a cell density of 60% –80%. After co-incubation for different time intervals (4, 12, and 24 h), the cell was washed with PBS three times and the fluorescence images of cells were obtained by CLSM (FV 1000, Olympus, Japan).

MTT Evaluation of the Cytotoxicity of Free DOX, DOX-IMNCs and DOX/CPT-IMNCs against MCF-7/ADR Cells: The in vitro cytotoxicity was evaluated by the typical 3-[4,5-dimethylthiazol-2-yl]-2,5-diphenyltetrazolium bromide (MTT) reduction assay. To evaluate the cytotoxicity of DOX/CPT-IMNCs against MCF-7/ADR cancer cells, MCF-7/ADR cells were seeded in a 96-well plate at a density of 5×10^3 per well and cultured in 5% CO_2 at 37 °C for 24 h. Free DOX, DOX-loaded IMNCs, and DOX/CPT-IMNCs were dispersed into the culture media (DMEM) with the equivalent DOX concentration by ultrasonic treatment, and the cells were incubated in 5% CO_2 at 37 °C for 24 or 48 h. The concentrations of DOX were 0, 1.25, 2.5, and 5 μg mL^{-1}, respectively. At the end of the incubation, the culture media were removed and 100 μL of MTT solutions (dissolved in DMEM with a finial concentration of 0.8 mg mL^{-1}) were added. The media were then replaced with 100 μL of dimethyl sulfoxide (DMSO) per well, and the absorbance was monitored by a microplate reader (Bio-TekELx800) at a wavelength of 490 nm. The cytotoxicity was expressed as the percentage of cell viability compared to untreated control cells. The cytotoxicity of IMNCs against MCF-7/ADR cells was assessed using a cell density of 1×10^4 per well with concentrations of 12.5, 25, 50, 100, 200, 400, 600, and 800 μg mL^{-1}.

Characterization: Transmission electron microscopy (TEM) images were acquired on a JEM-2100F electron microscope operating at 200 kV. Scanning electron microscopy (SEM) images were obtained on a field emission HITACHI S-4800 microscope. Ultraviolet/Visible (UV/Vis) spectra were recorded on a UV-3101PC Shimadzu spectroscope. Nitrogen adsorption–desorption isotherms at 77 K were measured on a Micrometitics Tristar 3000 system. Thermogravimetry (TG) curves were recorded on a Netzsch STA 449C microanalyzer in air flow at 10 K min^{-1}. HIFU experiment was carried out by a JC HIFU tumor therapy system (Chongqing Haifu Technology, Chian) combined with an ultrasound imaging system for in situ monitoring the therapeutic effect. The therapeutic and diagnostic frequency were 3.5 and 1.1 MHz, respectively, and the therapeutic transducer (diameter: 220 mm, focal length: 145 mm) was fixed at the bottom of a tank filled with degassed water.

Supporting Information

Supporting Information is available from the Wiley Online Library or from the author.

Acknowledgements

This work was supported by the National Basic Research Program of China (973 Program, Grant No. 2011CB707905, 2009CB930304, and 2010CB934000), Shanghai Rising-Star Program (Grant No. 10QH1402800), National Nature Science Foundation of China (Grant Nos. 51132009, 50823007, 51072212, 51102259), the Science and Technology Commission of Shanghai (Grant Nos. 11nm0506500, 10430712800), and the Science Foundation for Youth Scholar of State Key Laboratory of High Performance Ceramics and Superfine Microstructures (Grant No. SKL201001).

Received: August 30, 2011
Revised: November 8, 2011
Published online: February 2, 2012

[1] a) J. M. Rosenholm, E. Peuhu, J. E. Eriksson, C. Sahlgren, M. Linden, *Nano Lett.* **2009**, *9*, 3308; b) Y. J. Wang, Y. Yan, J. W. Cui, L. Hosta-Rigau, J. K. Heath, E. C. Nice, F. Caruso, *Adv. Mater.* **2010**, *22*, 4293; c) E. M. Merisko-Liversidge, G. G. Liversidge, *Toxicol. Pathol.* **2008**, *36*, 43.

[2] a) K. S. Cunha, M. L. Reguly, U. Graf, H. H. R. de Andrade, *Mutagenesis* **2002**, *17*, 141; b) J. Lu, M. Liong, J. I. Zink, F. Tamanoi, *Small* **2007**, *3*, 1341.

[3] a) T. M. Allen, P. R. Cullis, *Science* **2004**, *303*, 1818; b) C. L. Lay, H. Q. Liu, D. C. Wu, Y. Liu, *Chem. Eur. J.* **2010**, *16*, 3001; c) Z. Liu, J. T. Robinson, X. M. Sun, H. J. Dai, *J. Am. Chem. Soc.* **2008**, *130*, 10876; d) L. L. Li, F. Q. Tang, H. Y. Liu, T. L. Liu, N. J. Hao, D. Chen, X. Teng, J. Q. He, *ACS Nano* **2010**, *4*, 6874.

[4] a) S. Sivakumar, V. Bansal, C. Cortez, S. F. Chong, A. N. Zelikin, F. Caruso, *Adv. Mater.* **2009**, *21*, 1820; b) T. Lian, R. J. Y. Ho, *J. Pharm. Sci.* **2001**, *90*, 667; c)T. Nakashima, M. Shimizu, M. Kukizaki, *Adv. Drug Delivery Rev.* **2000**, *45*, 47.

[5] a) B. Fadeel, A. E. Garcia-Bennett, *Adv. Drug Delivery Rev.* **2010**, *62*, 362; b) A. S. Karakoti, S. Das, S. Thevuthasan, S. Seal, *Angew. Chem. Int. Ed.* **2011**, *50*, 1980; c) Q. J. He, J. L. Shi, *J. Mater. Chem.* **2011**, *21*, 5845; d) Y. Piao, A. Burns, J. Kim, U. Wiesner, T. Hyeon, *Adv. Funct. Mater.* **2008**, *18*, 3745.

[6] a) Y. Chen, H. R. Chen, L. M. Guo, Q. J. He, F. Chen, J. Zhou, J. W. Feng, J. L. Shi, *ACS Nano* **2010**, *4*, 529; b) Y. Chen, H. R. Chen, D. P. Zeng, Y. B. Tian, F. Chen, J. W. Feng, J. L. Shi, *ACS Nano* **2010**, *4*, 6001; c)Y. Chen, H. R. Chen, M. Ma, F. Chen, L. M. Guo, L. X. Zhang, J. L. Shi, *J. Mater. Chem.* **2011**, *21*, 5290.

[7] a) Y. Wan, D. Y. Zhao, *Chem. Rev.* **2007**, *107*, 2821; b) Y. Chen, H. R. Chen, S. J. Zhang, F. Chen, L. X. Zhang, J. M. Zhang, M. Zhu, H. X. Wu, L. M. Guo, J. W. Feng, J. L. Shi, *Adv. Funct. Mater.* **2011**, *21*, 270.

[8] a) M. Vallet-Regi, A. Ramila, R. P. del Real, J. Perez-Pariente, *Chem. Mater.* **2001**, *13*, 308; b) Y. F. Zhu, J. L. Shi, W. H. Shen, X. P. Dong, J. W. Feng, M. L. Ruan, Y. S. Li, *Angew. Chem. Int. Ed.* **2005**, *44*, 5083.

[9] a) Q. Zhang, T. R. Zhang, J. P. Ge, Y. D. Yin, *Nano Lett.* **2008**, *8*, 2867; b) S. J. Park, Y. J. Kim, *Langmuir* **2008**, *24*, 12134; c) W. Meier, *Chem. Soc. Rev.* **2000**, *29*, 295.

[10] a) D. Chen, L. L. Li, F. Q. Tang, S. O. Qi, *Adv. Mater.* **2009**, *21*, 3804; b) L. F. Tan, D. Chen, H. Y. Liu, F. Q. Tang, *Adv. Mater.* **2010**, *22*, 4885.

[11] T. R. Zhang, J. P. Ge, Y. X. Hu, Q. Zhang, S. Aloni, Y. D. Yin, *Angew. Chem. Int. Ed.* **2008**, *47*, 5806.

[12] a) S. D. Conner, S. L. Schmid, *Nature* **2003**, *422*, 37; b) M. Marsh, H. T. McMahon, *Science* **1999**, *285*, 215.

[13] a) J. E. Kennedy, G. R. ter Haar, D. Cranston, *Br. J. Radiol.* **2003**, *76*, 590; b) M. R. Bailey, V. A. Khokhlova, O. A. Sapozhnikov, S. G. Kargl, L. A. Crum, *Acoust. Phys.* **2003**, *49*, 369.

[14] Y. Kaneko, T. Maruyama, K. Takegami, T. Watanabe, H. Mitsui, K. Hanajiri, H. A. Nagawa, Y. Matsumoto, *Eur. Radiol.* **2005**, *15*, 1415.

[15] B. E. Oeffinger, M. A. Wheatley, *Ultrasonics* **2004**, *42*, 343.

[16] E. G. Schutt, D. H. Klein, R. M. Mattrey, J. G. Riess, *Angew. Chem. Int. Ed.* **2003**, *42*, 3218.

[17] S. M. Lee, T. V. O'Halloran, S. T. Nguyen, *J. Am. Chem. Soc.* **2010**, *132*, 17130.

[18] a) A. M. Chen, M. Zhang, D. G. Wei, D. Stueber, O. Taratula, T. Minko, H. X. He, *Small* **2009**, *5*, 2673; b) H. A. Meng, M. Liong, T. A. Xia, Z. X. Li, Z. X. Ji, J. I. Zink, A. E. Nel, *ACS Nano* **2010**, *4*, 4539.

[19] a) L. M. Zhang, J. G. Xia, Q. H. Zhao, L. W. Liu, Z. J. Zhang, *Small* **2010**, *6*, 537; b) S. Modok, H. R. Mellor, R. Callaghan, *Curr. Opin. Pharmacol.* **2006**, *6*, 350.